Technische Universität Berlin
Institut für Luft- und Raumfahrt
Fachgebiet Flugmechanik Flugregelung und Aeroelastizität

TECHNISCHE UNIVERSITÄT BERLIN

Flight Control

1. Homework

Analysis of dynamic aircraft behavior and design of a stability augmentation system

Betreuer

M.Sc. Henrik Spark

Group 3

Tang, Hoai Nam	XXXXXX
Bayer Botero, Federico	XXXXXX
Shalahuddin, Muhammad Nauval	XXXXXX
Nenejian, Harout	XXXXXX

Berlin, December 14, 2024

Contents

Analysis of Dynamic Aircraft Behavior and Design of a Stability Augmentation System

H. N. Tang, H. Nenejian, F. B. Bayer and N. M. Shalahuddin
Department of Flight Mechanics, Flight Control and Aeroelasticity,
Technische Universität Berlin, Marchstrasse 12, 10587 Berlin, Germany.

Modern conventional aircraft exhibits complex and coupled eigenmodes due to the aerodynamic design. This paper examines aircraft stability and flying quality characteristics as well as proposes the control solution for stability augmentation system. This solution is based only upon simple proportional feedback control scheme. Still, both linear and fully nonlinear flight simulation results demonstrate significant improvements in both longitudinal and lateral-directional motion while maintaining pilot control authority. Therefore, the implemented stability augmentation system will enhance aviation safety and reduce pilot workload, enabling pilots to focus on other critical flight management tasks.

I. Nomenclature

Symbols

α	=	angle of attack
f	=	frequency
$\delta a, \delta e, \delta r$	=	aileron, elevator, rudder deflection
δt	=	thrust input
F, G	=	transfer function
γ	=	flight-path angle
H	=	altitude
K	=	proportional gain
λ	=	eigenvalue of matrix
ω	=	angular frequency
ω_n	=	natural frequency
n	=	load factor
Φ, Θ, Ψ	=	bank, pitch, and yaw angle
p, q, r	=	roll, pitch, and yaw rate
σ	=	real part

T	=	time constant
T_2	=	doubling time
I	=	identity matrix
V	=	velocity
x, u, y, r	=	state, control input, output, and reference vector
ζ	=	damping ratio

Indices

cmd	=	command (reference) signal
PH, SP, R, DR, S	=	phugoid, short-period, pure roll, Dutch roll, and spiral mode
ol, cl	=	open loop, closed-loop control system
trim	=	trim (equilibrium) condition
wo	=	washout filter
∞	=	steady state

Abbreviations

ALT	=	Altitude
CAP	=	control anticipation parameter
c.g.	=	center of gravity
FQ	=	flying quality
FVT	=	final value theorem
LFS	=	load factor sensitivity
ROC	=	Rate of Climb
SAS	=	stability augmentation system

II. Introduction

Flying quality (FQ) and handling quality (HQ) are the crucial components in aircraft design. FQ encompasses aircraft's inherent stability and its response to control inputs and atmospheric disturbances, while HQ refers to pilot's subjective assessment of operational difficulties. Since FQ fundamentally influences HQ, they form the primary focus of aircraft certification requirements regarding flight characteristics. Aviation authorities have strict requirements to ensure safe, predictable, and satisfactory FQ under various operational conditions. One of the most well-known standards is the U.S. military specification MIL-F-8785C. Originally developed for military purposes, it was later applied to civil

aircraft and now serves as a key reference for analyzing flight characteristics. Due to the distinctive aerodynamic design, conventional aircraft often fail to meet these requirements. To achieve certification compliance, stability augmentation systems (SAS) are implemented to enhance aircraft stability and indirectly assist pilot control during operations.

This report is divided into four parts. The first part is analysis of eigenbehavior. The longitudinal and lateral-directional FQ of VFW 614 is analyzed from its linearized state space dynamic model. The analysis results will be evaluated against MIL-F-8785C specifications to assess compliance with flying quality requirements. The next section will be an examination of the longitudinal dynamics and the design of feedback controller to improve the flight characteristics of the pitch motion. A detailed analysis of the coupled lateral-directional dynamics and the design procedure of SAS for decoupling those modes are discussed in part three. As a regulator problem, for designing the SAS only proportional controller is used. We decided to not use the integral controller to avoid unnecessary delays. Finally, we will evaluate our analysis and our controllers in a nonlinear flight simulator. The flight simulation of the VFW 614 was conducted by students in the SEPHIR simulator of the Technische Universität Berlin.

III. Analysis of the eigenbehaviour

In this Analysis, we will examine the eigenbehavior of the VFW-614 aircraft for the given reference flight condition. The goal is to evaluate the aircraft's flying qualities, in order to design flight controler according to the requirements.The evaluation will be based on the military standard MIL-F-8785C, which classifies aircraft performance into three levels.:

- Level 1: The flying qualities are clearly adequate for the given flight mission.
- Level 2: The flying qualities are adequate for the given mission, but some increase in pilot workload or degradation in mission effectiveness, or both exist.
- Level 3: The flying qualities are such that the aircraft can be controlled safely, but pilot workload is excessive and mission effectiveness is inadequate, or both.

To start the analysis, the VFW-614 is a low-wing, short-range aircraft with two jet engines mounted above the wings. According to MIL-F-8785C, it is classified as a Class III aircraft (low-to-medium maneuverability). The reference state is stationary horizontal flight just before landing, at an altitude of 4000 feet and a speed of 180 knots. This phase is classified as terminal, which corresponds to Category C in MIL-F-8785C. The linearized state-space equation for longitudinal Motion and lateral movement is given as:

$$\begin{bmatrix} \delta\dot{q} \\ \delta\dot{\alpha} \\ \delta\dot{V} \\ \delta\dot{\Theta} \end{bmatrix} = \begin{bmatrix} -0.9981 & -2.5072 & -3.518\times10^{-4} & 0 \\ 0.9709 & -0.9632 & -0.0025 & 0.0099 \\ -0.1274 & 4.6526 & -0.0219 & -9.7234 \\ 1 & 0 & 0 & 0 \end{bmatrix} \begin{bmatrix} \delta q \\ \delta\alpha \\ \delta V \\ \delta\Theta \end{bmatrix} + \begin{bmatrix} 0.1335 & -5.6897 \\ -0.0048 & -0.1038 \\ 2.9885 & -0.6188 \\ 0 & 0.0518 \end{bmatrix} \begin{bmatrix} \delta t \\ \delta e \end{bmatrix} \tag{1}$$

$$\begin{bmatrix} \delta\dot{r} \\ \delta\dot{\beta} \\ \delta\dot{p} \\ \delta\dot{\Phi} \end{bmatrix} = \begin{bmatrix} -0.4956 & 1.9243 & -0.1206 & 0 \\ -0.9795 & -0.1930 & 0.0963 & 0.1055 \\ 2.1070 & -5.5049 & -3.3388 & 0 \\ 0 & 0 & 1 & 0 \end{bmatrix} \begin{bmatrix} \delta r \\ \delta\beta \\ \delta p \\ \delta\Phi \end{bmatrix} + \begin{bmatrix} -0.4515 & -1.3180 \\ 0 & 0.0362 \\ -9.4980 & 1.9929 \\ 0 & 0 \end{bmatrix} \begin{bmatrix} \delta a \\ \delta r \end{bmatrix} \tag{2}$$

A. Analysis I

Examinantion of the flight qualities using the MIL-F-8785C specification and fig. 2 in longitudinal and lateral-directional motion.

1. Longitudinal motion

The Longitudinal motion describes the movement around the Pitch-Axis $x_b - z_b$and involves changes in altitude and speed. The main controls in the Longitudinal motion are elevator δe and throttle δt. Starting the analysis of the longitudinal motion, it is necessary to examine the eigenmodes. These are defined by their Eigenvalues λ and eigenvectors, which are calculated using the characteristic polynomial of the system matrix. In first place this will be done for short Period and in the following with the phugoid mode.

$$0 = |A - \lambda I| \tag{3}$$

$$\lambda = \sigma \pm i \cdot \omega \tag{4}$$

After calculating the eigenvalues, which consist of a real part and an imaginary unit, it is possible to determine the natural frequency ω_n and damping of the System ζ.

$$\omega_n = \sqrt{\sigma^2 + \omega^2} \tag{5}$$

$$\zeta = -\frac{\sigma}{\omega_n} \tag{6}$$

Applied to the system matrix A for the longitudinal motion , the following values are obtained:

$$\lambda_{SP} = -0,9804 \pm i \cdot 1,5581 \tag{7}$$

$$\omega_{n,SP} = \sqrt{\sigma_{SP}^2 + \omega_{SP}^2} = 1.841\,\text{rad/s} \tag{8}$$

$$\zeta_{SP} = -\frac{\sigma_{SP}}{\omega_{n,SP}} = 0.533 \tag{9}$$

To verify the results of the Short Period Eigenvalues, this is done for an approximation of the Short Period. The system is simplified to two states: pitch rate $\dot{q}$ and angle of attack α, as these are the most relevant for the short period. Additionally, the inputs are reduced to just one, the elevator deflection δ_e, since the influence of thrust δ_t on the short period is insignificant. The state-space representation for the short period approximation is displayed as the next equation.:

$$\begin{pmatrix} \dot{\delta q} \\ \dot{\delta \alpha} \end{pmatrix} = \begin{pmatrix} -0.9981 & -2.5072 \\ 0.9709 & -0.9632 \end{pmatrix} \begin{pmatrix} \delta q \\ \delta \alpha \end{pmatrix} + \begin{pmatrix} -5.6897 \\ -0.1038 \end{pmatrix} \begin{pmatrix} \delta e \end{pmatrix} \tag{10}$$

$$\lambda_{SP,approx} = -0.9807 \pm i \cdot 1.5601 \tag{11}$$

$$\omega_{n,SP,approx} = \sqrt{\sigma_{SP,approx}^2 + \omega_{SP,approx}^2} = 1.843\,\text{rad/s} \tag{12}$$

$$\zeta_{SP,approx} = -\frac{\sigma_{SP,approx}}{\omega_{n,SP,approx}} = 0.532 \tag{13}$$

The next table shows the requirements for Short-Period. In this Case the requirements represent a minima and a maxima for the damping ratio of the Short Period Eigenmode.

Level	$\zeta_{SP,min}$	$\zeta_{SP,max}$
1	0.35	1.30
2	0.25	2.00
3	0.15	-

Table 1 Short-period damping ratio limits for category C flight phases (MIL-F-8785C - 3.3.2.1.2)

Comparing them to the results calculated it shows both, Short Period and Short Period Approximation, meet the requirements of damping ratios. In conclusion, it can be said that the approximation of the Short Period, due to the similarity of the results to the actual Short Period, shows that the influence of V and Theta on this eigenmode is negligible.

To fully investigate the entire longitudinal motion according to MIL-F-8785C and address the question of stability

of the eigenmodes, the phugoid mode must also be considered.

$$\lambda_{PH} = -0,0112 \pm i \cdot 0,1306 \tag{14}$$

$$\omega_{n,PH} = \sqrt{\sigma_{PH}^2 + \omega_{PH}^2} = 0.1311 \text{ rad/s} \tag{15}$$

$$\zeta_{PH} = -\frac{\sigma_{PH}}{\omega_{n,PH}} = 0.0856 \tag{16}$$

The following table shows the requirements for minimal damping ratio for phygoid mode.

Level	$\zeta_{PH,min}$
1	0.04
2	0
3	$T_{2,PH,min} \geq 55$ s

Table 2 Minimum damping ratio for the phugoid (MIL-F-8785C - 3.2.1.2)

The table 2 shows, that the phugoid mode with a damping ratio of $\zeta_{PH} = 0.0856$ meets the requirements for Level 1 for the phugoid mode.

In order to verify the calculated results graficly. Both eigenmodes are displayed in the complex lane.

From the representation of the eigenvalue pairs in the complex plane, it can be concluded that the displayed eigenmodes are stable due to their negative real part. Additionally, it is evident that the Short Period eigenmode and its approximation are relatively high-frequency with high damping. In contrast, the Phugoid mode is a slow oscillating eigenmode with weak damping.

The next parameter regarding the short period that must meet the MIL-F-8785C standard is the limit for the Control Anticipation Parameter (CAP). The Controll Anticipation Parameter (CAP) is characterised by the response of an Aircraft to an elevator input.

The CAP is defined as the ratio of the initial pitch acceleration $\left(\delta p\big|_{t=0}\right)$ to the steady-state load factor $\left(\delta n_z\big|_{t\to\infty}\right)$.

$$\text{CAP} = \frac{\dot{\delta p}\big|_{t=0}}{\delta n_z\big|_{t\to\infty}} = \frac{\omega_n^2}{\delta n_z} \cdot \frac{\delta\alpha}{\delta\alpha} \tag{17}$$

To analyze the CAP, it is necessary to introduce the Load Factor Sensitivity (LFS). The LFS describes the changes in the load factor due to variations in the angle of attack.

Using the LFS, the CAP can be expressed as follows, assuming $\gamma = 0°$, resulting in the values for the Short Period Mode and the approximation.

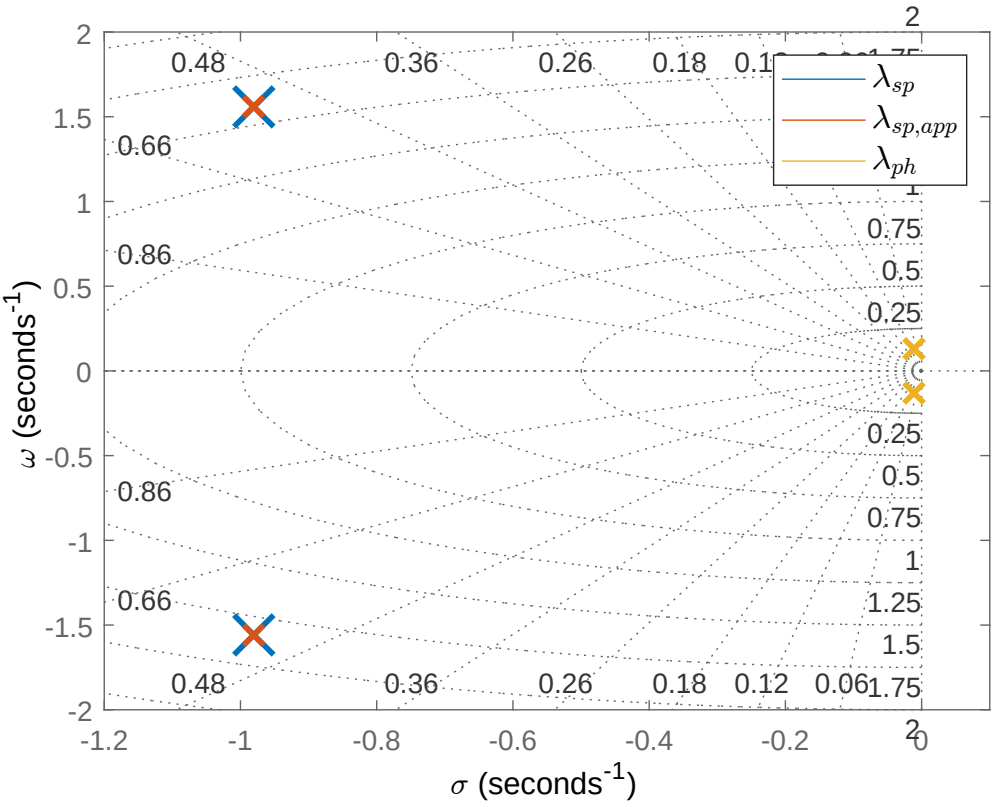

Fig. 1 Eigenvalues of the longitudinal motion in the complex plane

$$\text{LFS} = \frac{\delta n_z}{\delta \alpha} = -\frac{V_r}{g} \cdot Z_\alpha \tag{18}$$

$$\text{CAP} = -\frac{g}{V_r} \cdot Z_\alpha \cdot \omega_n^2 \tag{19}$$

In the following figure, the calculated CAP values are plotted in the corresponding plot for CAP limitations. Both modes comply with the requirements for Level 1 of the MIL-F-8785C.

As the last task to analyze longitudinal motion, it is necessary to evalute the so called „Fingerprint Plot“. The Fingerprint Plot is a tool used to check the aircraft stability and controls and to ensure a safe and predictable flight behavior. „The Fingerprint-Plot“ is divided in several categories from Unacceptable to Satisfactory.

The performance oft he VFW-614 is located in the poor Region. This goes along with large control inputs and slow responses and would need to be improved by designing the controller.

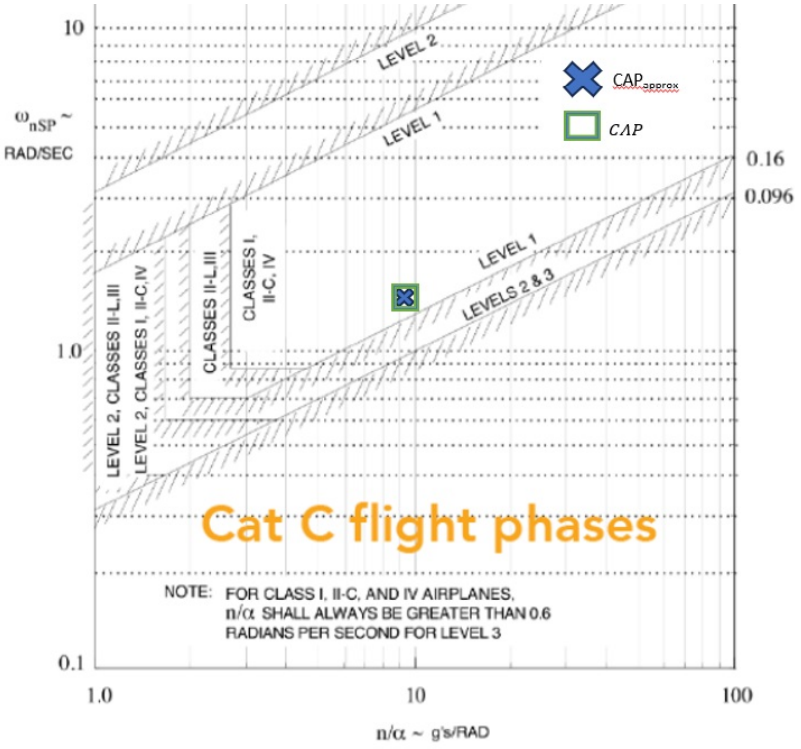

Fig. 2 CAP limitations (MIL-F-8785C - 3.2.2.1.1)

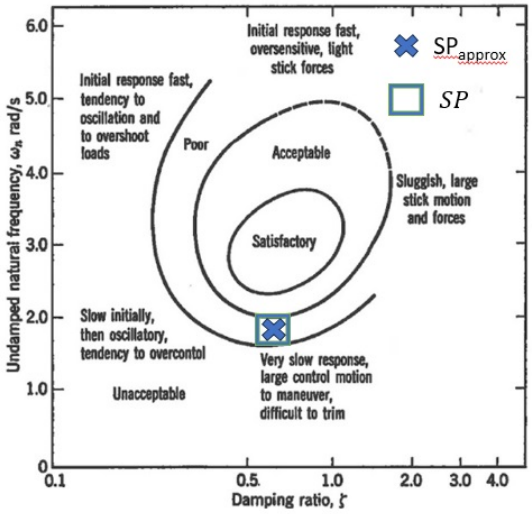

Fig. 3 "Fingerprint Plot"

2. Lateral movement

The lateral movement describes movements rotating around the yaw axis and roll axis. The main controls in the longitudinal motion are ailerons δ_a and rudder δ_r. The lateral movement is essential for controlling the direction

and stability and includes three eigenmodes: Dutch roll (DR), spiral (S), and pure roll (R), which are analyzed in the following task.

Their eigenvalues can be calculated with the system matrix for lateral movement $A_{\text{lat}}(2)$.

$$\lambda_{\text{DR}} = -0.4188 \pm i \cdot 1.5079 \tag{20}$$

$$\lambda_{\text{R}} = -3.2076 \tag{21}$$

$$\lambda_{\text{S}} = 0.0178 \tag{22}$$

As with the longitudinal motion and the Short Period eigenmode, an approximation matrix is also used for the Dutch roll here. Since the Dutch roll can be seen as a coupled oscillatory motion, in which the rudder δr is the dominating influence. The Dutch roll approximation can be written as:

$$\dot{x}_{\text{DR,approx}} = \begin{bmatrix} -0.4956 & 1.9243 \\ -0.9795 & -0.1930 \end{bmatrix} \dot{x}_{\text{DR,approx}} + \begin{bmatrix} -1.3118 \\ 0.0362 \end{bmatrix} u_{\text{DR,approx}} \tag{23}$$

$$\lambda_{\text{DR,approx}} = -0.3443 \pm i \cdot 1.3645 \tag{24}$$

The following figure shows the eigenvalues of the corresponding eigenmodes. The dutch roll and its approximation show a high natural frquency ω_n paired with low damping Ratio ζ. It also shows that the approximation of dutch roll has still similiar charakteristicas like the regular one, but their eigenvalues are not so close compared to the short period eigenmode. Pure roll and spiral represent aperiodic eigenmodes with no imaginary unit. The pure roll motion is characterized as a slow and stable mode, with a highly negative eigenvalue. In contrast, the spiral mode has a slightly positive eigenvalue and is therefore slightly unstable.

In the following, after examining the basic characteristics of lateral movement, the spiral, pure roll, and Dutch roll modes are further investigated to ensure compliance with MIL-F-8785C.

The spiral mode is characterized as an aperiodic mode, influenced primarly by the roll angle and slideslip angle. In Order to comply with MIL-F-8785C the spiral mode must meet a provided value regarding the doubling time as shown in the following table:

To calculate the doubling time, the natural frequency is used:

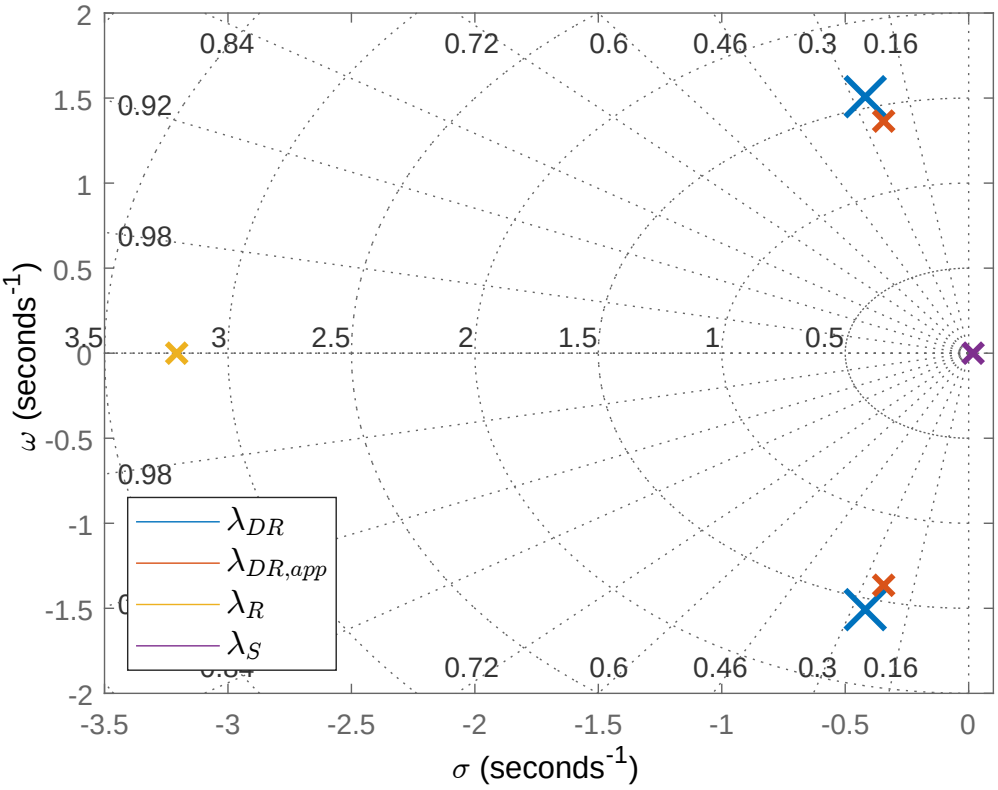

Fig. 4 Eigenvalues of the lateral movement in the complex plane

Level	T2,S,min [s]
1	12
2	8
3	4

Table 3 Minimum time to double amplitude for the spiral mode in category C flight phases (MIL-F-8785C - 3.3.1.3)

$$T_{2,S} = \frac{\ln(2)}{\omega_{n,S}} = \frac{\ln(2)}{0.0178} \approx 38.9\,\text{s} \tag{25}$$

The spiral mode meets the requirements for Level 1 of the MIL-F-8785C standard.

As described before, the pure roll is an aperiodic mode around the x_b-axis. The MIL-F-8785C describes two requirements for the pure roll mode. The first one describes a maximum of roll mode time constant. Where T_R is the time it takes to reach 67% of the steady-state roll rate after a step input on the ailerons. The second criterion is to determine the time required for the pure roll mode to achieve a 30° change in bank angle.

In order to investigate the first criterion, we take a look at the lateral movement state space and use the roll-equation [**?**].

Level	T_R,max [s]
1	1.4
2	3.0
3	10

Table 4 Maximum roll time constant for category C flight phases (MIL-F-8785C - 3.3.1.2).

Level	t_{max} [s]
1	2.5
2	4.0
3	6.0

Table 5 Time limits to achieve a 30° bank angle for a class III aircraft in category C flight phases (MIL-F-8785C - 3.3.4.2).

$$\delta\dot{p} = L_p \cdot \delta p + L_{\delta a} \cdot \delta\delta a \tag{26}$$

To apply the rule, we first take the Laplace transform of the equation and then convert it into PT1 form.

$$\delta p(s) = \frac{-L_{\delta a}}{L_p} \cdot \frac{1}{TR \cdot s + 1} \cdot \delta\delta a(s) \tag{27}$$

Looking at the equation , it is clear that the time constant is the inverse of the absolute value of the eigenvalue.

$$T_{R,\text{approx}} = \frac{1}{|L_p|} \quad \Rightarrow \quad T_R = \frac{1}{|\lambda_R|} \approx 0.3\,\text{s} \tag{28}$$

The time constant complies with Level 1 of MIL-F-8785C.

For the second criterion, the time needed to achieve a 30° roll angle Change, the answer for a step Input is needed and displayed in the following:

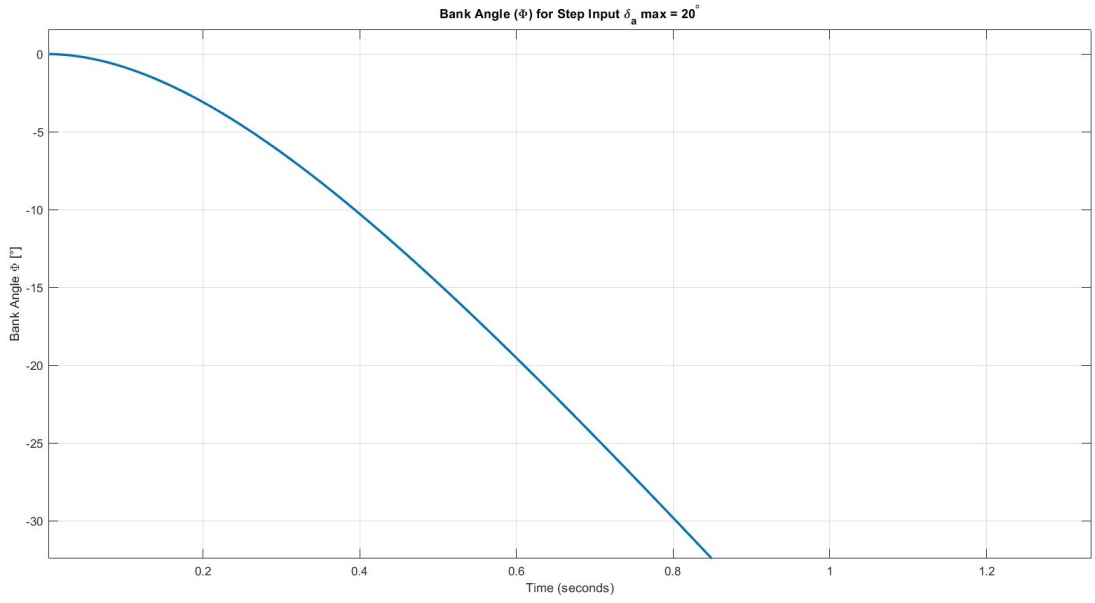

Fig. 5 Bank angle for a step input.

It shows that the time necessary to achieve 30° is around 0.8 seconds, and therefore meets Level 1 requirements.

The final step in analyzing the pure roll eigenmode is assessing the effectiveness of the ailerons. To assess aileron effectiveness, we need to calculate two important values in the Laplace domain: the initial roll acceleration $\dot{p}(t = 0)$ and the steady-state roll rate p_∞. These can be determined using the initial value theorem (IVT) and the final value theorem (FVT).

$$\dot{p}(t = 0) = \lim_{s \to \infty} s \cdot F_{p,\delta a}(s) \tag{29}$$

With the initial roll acceleration $\dot{p}(t = 0) = \lim_{s\to\infty} s \cdot F_{p,\delta a}(s)$, where $F_{p,\delta a}(s)$ is the transfer function from aileron deflections δa to roll rate p. The result gives an approximation for the initial roll acceleration:

$$\dot{\delta p}\Big|_{t=0} = \lim_{s \to \infty} s \cdot \frac{\delta\delta a, \max}{s} \cdot \left(s \cdot \frac{\delta p}{\delta\delta a}(s) \right) \Bigg|_{\mathrm{F}_{p,\delta a}} = L_{\delta a} \cdot \delta a_{\max} \approx -190^\circ \, \mathrm{s}^{-2} \tag{30}$$

The Final Value Theorem (FVT) is used to calculate the steady-state roll rate:

$$\dot{\delta p}_\infty = \lim_{s \to 0} s \cdot \frac{\delta\delta a_{\max}}{s} \cdot \left(s \cdot \frac{\delta p}{\delta\delta a}(s) \right) \Bigg|_{F_{p,\delta a}} = -\frac{L_{\delta a}}{L_{\delta p}} \cdot \delta a_{\max} = T_R \cdot \dot{p}|_{t=0} \approx -59^\circ / s^2 \tag{31}$$

We can then calculate the bank angle change $\delta\Phi(t)$ as a function of the roll time constant T_R and the initial roll acceleration $\delta\dot{p}|_{t=0}$.

$$\delta\Phi(t) = T_R \cdot \dot{p}(t = 0) \cdot \left(t - T_R \cdot \left(1 - \frac{t}{T_R} \right) \right) \tag{32}$$

By calculating the initial roll acceleration and steady-state roll rate, we can assess the aileron effectiveness of the aircraft. In this case, for the VFW-614, the aileron effectiveness is in the "Level 2" region, which is satisfactory but could be improved.

In summary, the aileron effectiveness is determined by the initial roll acceleration, the steady-state roll rate, and the roll time constant T_R. These calculations help determine how effectively the aircraft responds to aileron inputs.

As the final step in analyzing the lateral dynamics, we will examine whether the Dutch Roll mode complies with the MIL-F-8785C Standards. The MIL-F-8785C standard requires minimum values for the damping ratio (ζ) and the natural frequency (ω_n).

Therefore we must calculate the natural frequency and damping for the dutch roll.

$$\omega_{n,DR} = \sqrt{\sigma_{DR}^2 + \omega_{DR}^2} = 1.57 \, \mathrm{rad/s} \tag{33}$$

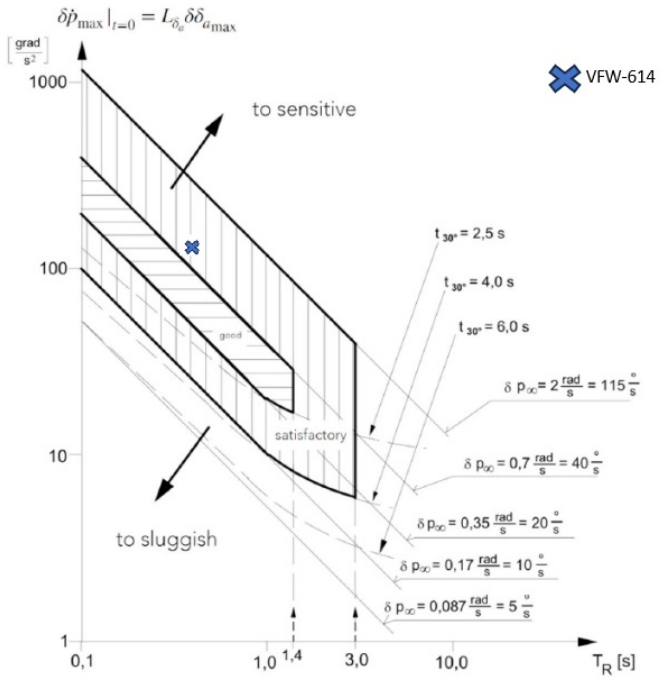

Fig. 6 "Aileron effectiveness"

Level	$\zeta_{DR,min}$	$(\zeta \cdot \omega_n)_{DR,min}$ [rad/s]	$\omega_{n,DR,min}$ [rad/s]
1	0.08	0.1	0.4
2	0.02	0.05	0.4
3	0	-	0.4

Table 6 Dutch roll stability requirements for category C flight phases (MIL-F-8785C -3.3.1.1)

$$\omega_{n,DR,approx} = \sqrt{\sigma_{DR,approx}^2 + \omega_{DR,approx}^2} = 1.41 \text{ rad/s} \tag{34}$$

$$\zeta_{DR} = \frac{-\sigma_{DR}}{\omega_{n,DR}} = 0.268 \tag{35}$$

$$\zeta_{DR,approx} = \frac{-\sigma_{DR,approx}}{\omega_{n,DR,approx}} = 0.245 \tag{36}$$

The calculated values Show, that both meet dutch roll Motion criterias for Level 1 MIL-F-8785C.

B. Analysis II

The second task is an analysis of the non-minimum phase behavior of the aircraft for thrust δ_t and elevator δ_e. The analysis of non-minimum phase behavior is required in order to be able to apply feedback and prevent the system from destabilizing. This behavior occurs when a stable pole becomes unstable through a gain factor.

The longitudinal motion consists of four states (q, α, V, Θ) and two inputs (δ_t, δ_e). Therefore, eight transfer functions must exist: $F_{p,\delta t}$, $F_{\alpha,\delta t}$, $F_{V,\delta t}$, $F_{\Theta,\delta t}$, $F_{p,\delta e}$, $F_{\alpha,\delta e}$, $F_{V,\delta e}$, and $F_{\Theta,\delta e}$.

In order to check whether non-minimum phase behavior exists, we first examine the poles and zeros of the transfer functions. Afterwards, we will analyze the time response of the transfer function.

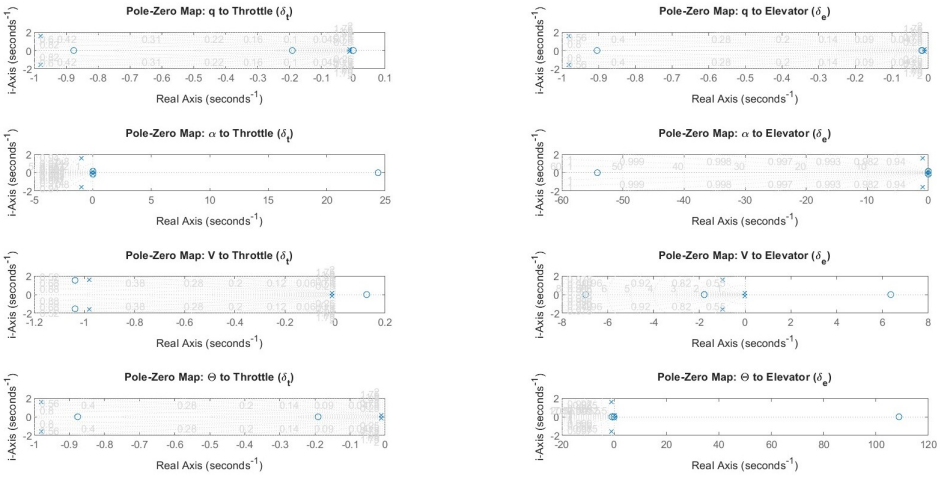

Fig. 7 Pole zero maps for transfer functions in the longitudinal motion

Revising the pole-zero maps indicates non-minimum-phase behavior for the following transfer functions: $F_{\alpha\rightarrow\delta t}$, $F_{V\rightarrow\delta e}$, and $F_{V\rightarrow\Theta}$.The same can be observed by analyzing the time responses to the individual step Inputs. The destabilizing characteristics of the non-minimum phase behavior must be taken into account when designing the controller.

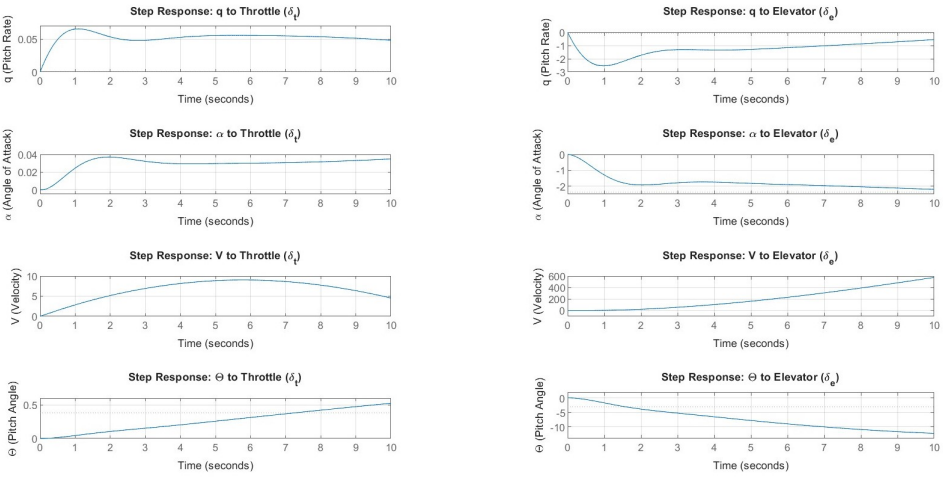

Fig. 8 Time response for a step input

C. Requirements for the controller design

Based on the analysis presented in Sections 1.1 and 1.2, the requirements for the controller design outlined in Section 2 will be derived, considering the controller's eigendynamics. The objective is to design a controller capable of achieving level 1 flight performance, as defined by the MIL-F-8785C standard, across all aspects of the preceding analysis. Therefore the following requirements should be taken into consideration:

- The VFW-614 aircraft already satisfies level 1 compliance under the standard for the following eigenmodes: Phugoid, Dutch roll mode, and Spiral mode. Consequently, the primary requirement for the controller is to preserve the level 1 flight performance of these modes, as no further performance enhancement is required.
- The second requirement for the controller is to adjust the natural frequency and damping of the short-period mode to achieve the optimal values indicated on the "Fingerprint Plot" ($\omega_{n,opt} = 0,3\frac{rad}{s}; \zeta_{opt} = 0,7$).
- Additionally, the roll time constant should be reduced to $T_R \leq 0,21s$ to achieve level 1 performance in this category. However, since the roll performance is already satisfactory, this requirement is optional and not mandatory. As such, lowering the roll time constant is recommended but not essential.

A summary of those requirements is provided in table 7

No.	Mode	Requirement	Compliance
1	PH	Maintain level 1 flight performance: $\zeta_{PH} \geq 0,04$	Mandatory
2	SP	Improve values of natural frequency and damping ratio to: $\omega_{n,opt} = 0,3\frac{rad}{s}; \quad \zeta_{opt} = 0,7$	Mandatory
3	DR	Maintain level 1 flight performance: $\zeta_{DR} \geq 0,08; \quad \omega_{n,DR} \geq 0,4\frac{rad}{s}; \quad \zeta_{DR} \cdot \omega_{n,DR} \geq 0,1\frac{rad}{s}$	Mandatory
4	R	Improve value of roll time constant to $T_R \leq 0,21s$	Optional
5	S	Maintain level 1 flight performance: $T_{2,S} \geq 12s$	Mandatory

Table 7 Design requirements for the fight controller to achieve level 1 flight performance in all longitudinal and lateral-directional modes

IV. Design of a flight controller with damper support in the longitudinal motion (SAS)

In this section, the effects of controller design for short-period mode and phugoid mode of the longitudinal motion will be discussed.

A. Architecture

To start the second task, we need to propose a general block diagram which represents a manual flight control with damper support, often called a SAS (Stability Augmentation System). The design of the block diagram is shown in Figure 9 below.

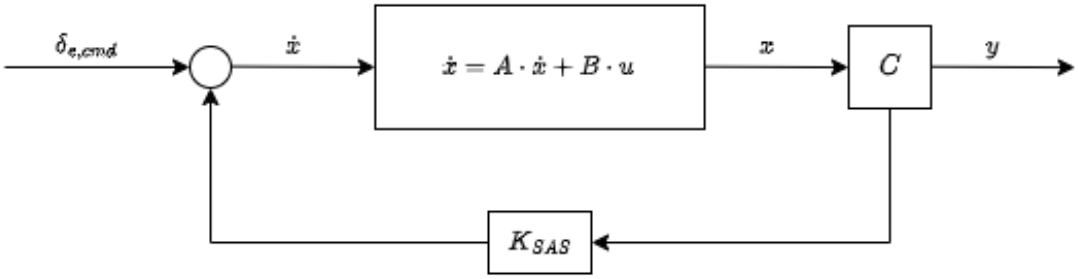

Fig. 9 General block diagram for manual flight control with damper support (SAS)

B. Controller Design I

In this part, we are trying to approximate the short-period mode of the longitudinal motion by means of analytical calculation. The equation for this approximation is shown below.

$$\begin{bmatrix} \delta\dot{q} \\ \delta\dot{\alpha} \end{bmatrix} = \underbrace{\begin{bmatrix} M_q' + M_{\dot{\alpha}} & M_\alpha' \\ Z_q + 1 & Z_\alpha \end{bmatrix}}_{A_{SP}} \begin{bmatrix} \delta_q \\ \delta_\alpha \end{bmatrix} + \underbrace{\begin{bmatrix} M_{\delta_e}' \\ Z_{\delta_e} \end{bmatrix}}_{B_{SP}} \delta_e \tag{37}$$

For the first controller, a pitch damper must be designed to achieve a degree of damping of the short-period mode of 0.7. This can be achieved by feeding back the pitch rate q with a certain gain K_q to the elevator deflection δ_e. We start by analyzing the closed-loop transfer function of the plant with feedback given in Equation 38.

$$F_{cl} = \frac{F_{q\delta_e}}{1 + K_q \cdot F_{q\delta_e}} \tag{38}$$

The transfer function $F_{q\delta_e}$ given by the input δ_e to the output q can be determined through Matlab and given in Equation 39.

$$F_{q\delta_e} = \frac{-5.69s - 5.22}{s^2 + 1.961s + 3.396} \tag{39}$$

By inserting Equation 39 in 38, we obtain the closed-loop transfer function of the controller as shown in Equation 40.

$$F_{cl} = \frac{-5.69s - 5.22}{s^2 + (1.961 - 5.69 \cdot K_q)s + (3.396 - 5.22 \cdot K_q)} \tag{40}$$

The denominator is a characteristic quadratic equation for oscillation, which can also be represented in the form given in Equation 41.

$$s^2 + 2 \cdot D \cdot \omega_n \cdot s + {\omega_n}^2 = 0 \tag{41}$$

Through coefficient comparison, we can define Equation 42 and 43.

$$D = \frac{1.961 - 5.69 \cdot K_q}{2 \cdot \omega_n} \tag{42}$$

$${\omega_n}^2 = 3.396 - 5.22 \cdot K_q \tag{43}$$

The objective of this controller design is a damping D of 0.7. By solving the two previous equations, it resulted to gain K_q of -0.1621 to achieve the desired target.

The corresponding controller design is shown in Figure 10.

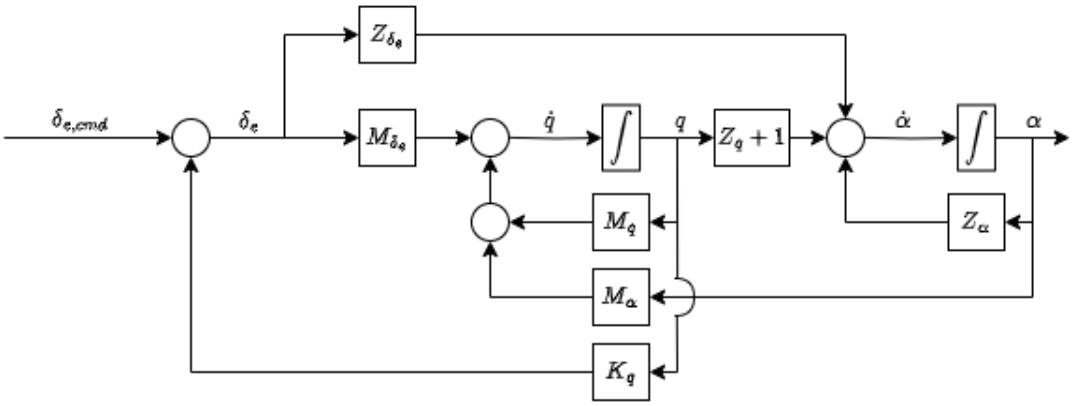

Fig. 10 Block diagram of short-period approximation with integrated pitch damper

C. Controller Design II

The damping and the natural frequency of the short-period mode can also be modified by means of the full state feedback in its approximation equation as already shown in Equation 37. To measure the states α and q, the aircraft utilizes respectively the Angle-of-Attack probe and the inertial measurement unit. The requirements for this controller are a damping ratio D of 0.7 and an undamped natural frequency f_0 of 0.4775 Hz.

To calculate gains with full state feedback, we can perform the analytical method of the so called pole placement. This method enables us to determine the gain sufficed for the objectives above. We need to make sure that the approximated state space allows this method to be used by checking the $rank$ of the controllability matrix. The controllability matrix Q_c is defined as

$$Q_c = [B_{SP} | A_{SP} \cdot B_{SP}] \tag{44}$$

$$Q_c = \begin{bmatrix} -5.6897 & 5.9391 \\ -0.1038 & -5.4241 \end{bmatrix} \tag{45}$$

and the $rank$ of this Q_c matrix is 2, which is the same as the number of input controls in our A_{SP}. We want to do the calculation in controllable canonical form which requires T matrix for the transformation. To have the T matrix, we first need to create the inverted T matrix with the following form.

$$T^{-1} = \begin{bmatrix} {e_n}^T \\ {e_n}^T \cdot A_{SP} \end{bmatrix} \tag{46}$$

The ${e_n}^T$ is the last element in the inverted Q_c matrix. This gives us the T matrix of

$$T = \begin{bmatrix} -5.2201 & -5.6897 \\ -5.6277 & -0.1038 \end{bmatrix}. \tag{47}$$

With the given T and T^{-1}, we can calculate our A_{SP} written in controllable canonical form.

$$A_{SP,T} = T^{-1} \cdot A_{SP} \cdot T \tag{48}$$

$$A_{SP,T} = \begin{bmatrix} 0 & 1 \\ -3.3956 & -1.9613 \end{bmatrix} \tag{49}$$

The last row in $A_{SP,T}$ matrix contains the characteristic coefficients of the characteristic polynomial of this state space.

$$\lambda^2 - 1.9613 \cdot \lambda - 3.3956 = 0 \tag{50}$$

The location of the desired pole is to be determined by its imaginary and real axis. The location along the imaginary axis is represented by the damping coefficient θ and the damped frequency ω defines the position along the real axis. With the given requirements of damping D of 0.7 and undamped frequency of f_0 of 0.4775 Hz, the desired pole locations or eigenvalues are

$$\begin{bmatrix} -D \cdot \omega_n + i \cdot \omega_n \cdot \sqrt{1 - D^2} & -D \cdot \omega_n - i \cdot \omega_n \cdot \sqrt{1 - D^2} \end{bmatrix} \tag{51}$$

with the corresponding characteristic polynomial equation of

$$\lambda^2 + 4.2003 \cdot \lambda + 9.0013 = 0. \tag{52}$$

Since both polynomial equation in Equation 50 and Equation 52 have the same number of coefficient, we can do coefficient comparison to determine the gain in controllable canonical form to achieve the requirement by its difference, which needs to be transformed back to the original form by applying transformation with T matrix.

$$K_T = \begin{bmatrix} 5.6057 & 2.2390 \end{bmatrix} \tag{53}$$

$$K = \begin{bmatrix} K_q & K_\alpha \end{bmatrix} = \begin{bmatrix} -0.3818 & 0.6419 \end{bmatrix} \tag{54}$$

The block diagram with integrated full state feedback controller is given in Figure 11.

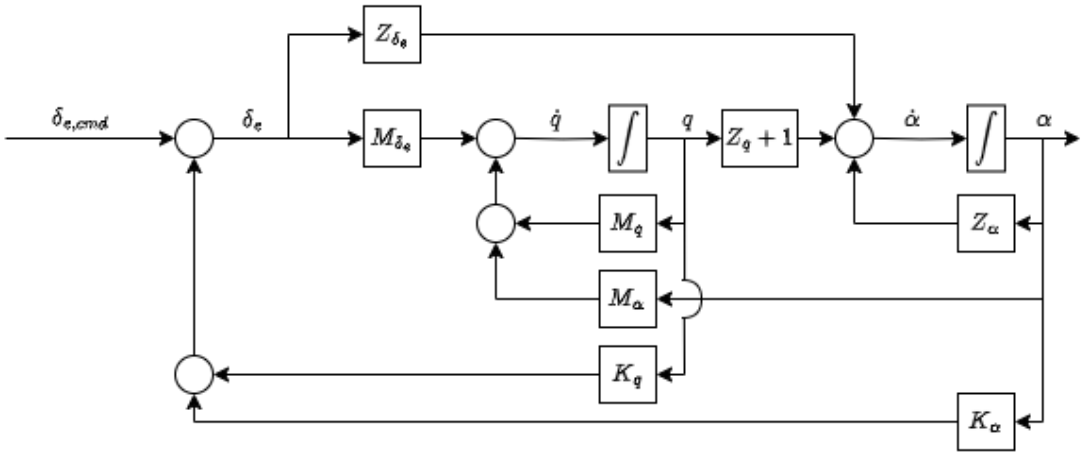

Fig. 11 Block diagram of short-period approximation with full state feedback controller

D. Verification I

To check the result of the designed both controller with only q feedback and full state feedback, a step on elevator will be used to simulate short-term and long-term responses on every state in the complete system of equations.

Both controller designs manage to suppress the oscillations coming from the step on the elevator, resulting in a lower magnitude of oscillation in every state. Looking at the short-period mode in Figure 12a, we can see that the oscillation of q and α will be damped in around 3 seconds without integrated controller, but only in around 1.5 seconds with full state feedback controller. The same effect can also be seen in the long-term phugoid mode, where the magnitudes of the oscillations are significantly lower compared to the system without a controller.

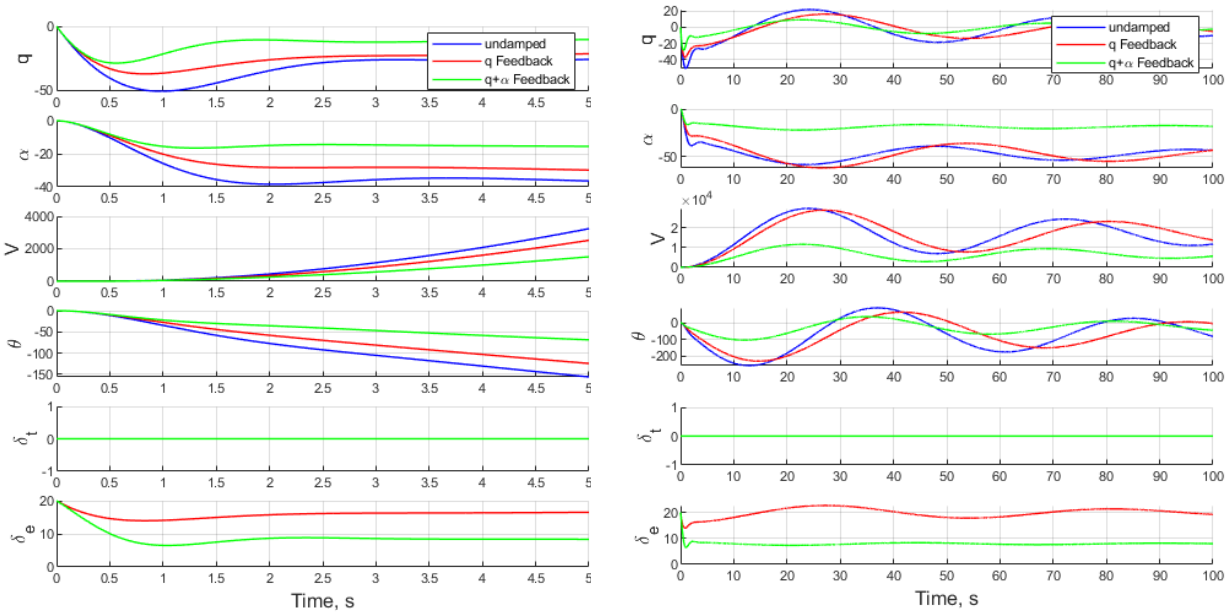

(a) Short-term simulation **(b) Long-term simulation**

Fig. 12 simulation with step on elevator δ_e

E. Controller Design III

In this section, a controller for phugoid damper must be designed. One can achieve this through feeding back the speed V to the thrust δ_t. The phugoid damper must be applied to the modified state space with a full state feedback in previous section.

$$A_{mod} = \begin{bmatrix} -3.1705 & -6.1596 & -0.0004 & 0 \\ 0.9313 & -1.0298 & -0.0025 & 0.0099 \\ -0.1274 & 4.6526 & -0.0219 & -9.7234 \\ 1.0000 & 0 & 0 & 0 \end{bmatrix} \tag{55}$$

The target of this phugoid damper is to have a damping D of 0.707. One method to look for sufficient gain is to go through the root locus diagram and see which gain meets our expectation.

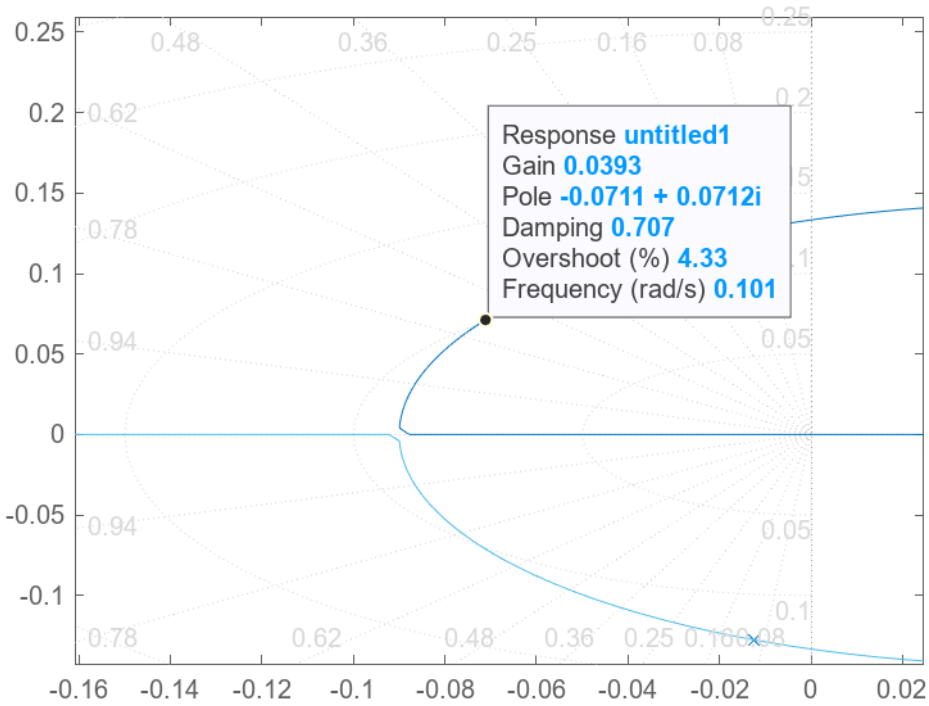

Fig. 13 Determining gain for damping D of 0.707

From the root locus diagram in Figure 13, the sufficient gain for the phugoid damper is 0.0393.

F. Verification II

After the integration of the phugoid damper into the modified state space A_{mod}, we simulate a step on elevator to see the response in a long term.

In Figure 14 we can see that the oscillations in two main states of phugoid mode V and θ, can be damped quicker compared to a system without phugoid damper. This can be achieved since the thrust is automatically adjusted by the damper. Since the phugoid is mainly influenced by the speed V and the pitch angle θ, a certain derivation in speed is damped by the phugoid damper.

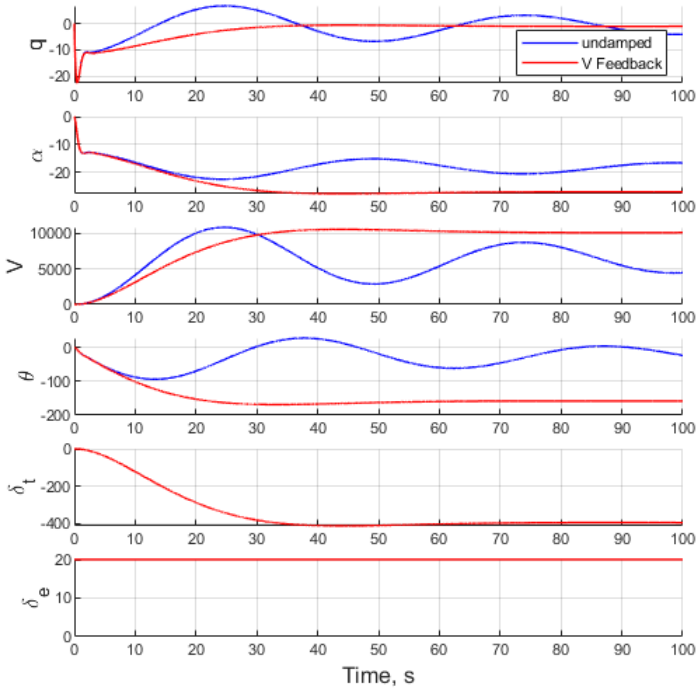

Fig. 14 Long-term simulation with step on elevator δ_e

V. Design of a base controller for decoupling lateral aircraft movement (SAS)

Due to aerodynamic design and asymmetric nature of fixed, swept-wing aircraft the lateral-directional dynamics demonstrates very strong coupling between yaw and roll motion. Since this coupling degrades the FQ of the aircraft and other essential functions, such as navigation, pilot workload is increased tremendously. Therefore, it is considered highly objectionable. To improve FQ, an SAS for the lateral-directional motion is to be designed. In the first step a yaw damper will be dimensioned to dampen the Dutch roll mode. Then, SAS will be improved to achieve sideslip-free turn.

A. Controller Design

The analysis of the eigenbehavior in Section III has shown that the Dutch roll motion is equivalent to FQ level 1 according to [1]. However, to further enhance the FQ, a yaw damper was designed to increase the Dutch roll damping ratio to 0.7. The rudder has more effects on yawing moment than the aileron, since $\left|N_{\delta_r}\right| > \left|N_{\delta_a}\right|$. Therefore, the yaw-rate-to-rudder feedback will result in a small, feasible feedback gain. Applying the root locus technique, we obtain a gain of -1.033, which implies positive feedback. In addition to Dutch roll characteristics improvement, this type of feedback also stabilizes the spiral mode. Figure 15 illustrates the improved lateral-directional response to a 5° rudder doublet input as a result of the yaw damper.

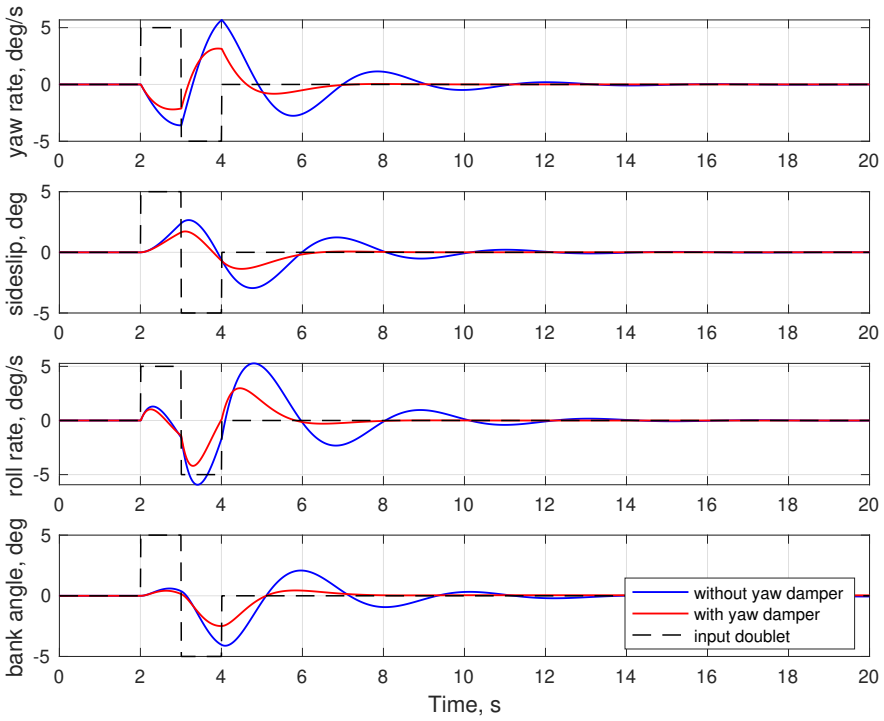

Fig. 15 Comparison of doublet response with and without yaw damper.

B. Intended Turn with Yaw Damper - Problem and Solution

The purpose of the yaw damper feedback is to use the rudder to generate a yawing moment that opposes any yaw rate that builds up from the Dutch roll mode. However, in coordinated turn, the yaw rate has a constant nonzero value which the yaw-rate feedback will try to oppose. Thus, with the yaw damper operating, the pilot must apply larger than normal rudder inputs to overcome the action of the yaw damper and coordinate a turn. A simple control system solution to the problem is to use "transient rate feedback," in which the feedback signal is approximately differentiated so that it vanishes during steady-state conditions and consequently nullifies the yaw damper's effectiveness. The approximate differentiation can be accomplished with a simple first-order high-pass filter, called a washout filter in this kind of application [2]. The block diagram of the yaw damper configuration with an integrated washout filter in the feedback loop is presented in Fig. 16.

The Dutch roll oscillation typically occurs at the frequencies exceeding those of pilot control inputs. Therefore, the yaw damper should activate at the Dutch roll natural frequency, while being suppressed at lower frequencies to preserve pilot authority over yaw control maneuver. The washout filter time constant, τ_{wo}, was configured to 4 s to achieve a good balance between performance and stability.

$$G_{\text{wo}} = \frac{\tau_{\text{wo}} s}{\tau_{\text{wo}} s + 1} = \frac{4s}{4s + 1} \tag{56}$$

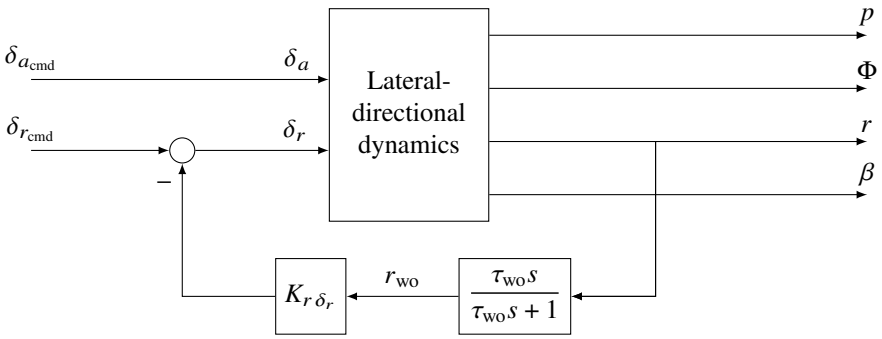

Fig. 16 Yaw damper.

Figure 17 illustrates the Bode diagram of the lateral-directional dynamics from rudder to yaw rate, the washout filter, and the resulted washed-out yaw rate, which will be fed back to the proportional controller to complete the yaw damper system. At low frequencies corresponding to typical pilot inputs, the resulted washed-out yaw rate is attenuated significantly. This implies the ineffectiveness of the yaw damper and full authority for the pilots. As the frequency approaches the Dutch roll damped frequency (the peak in Fig. 17), the washed-out yaw rate converges with the aircraft's lateral-directional dynamics and the yaw damper will come into effect.

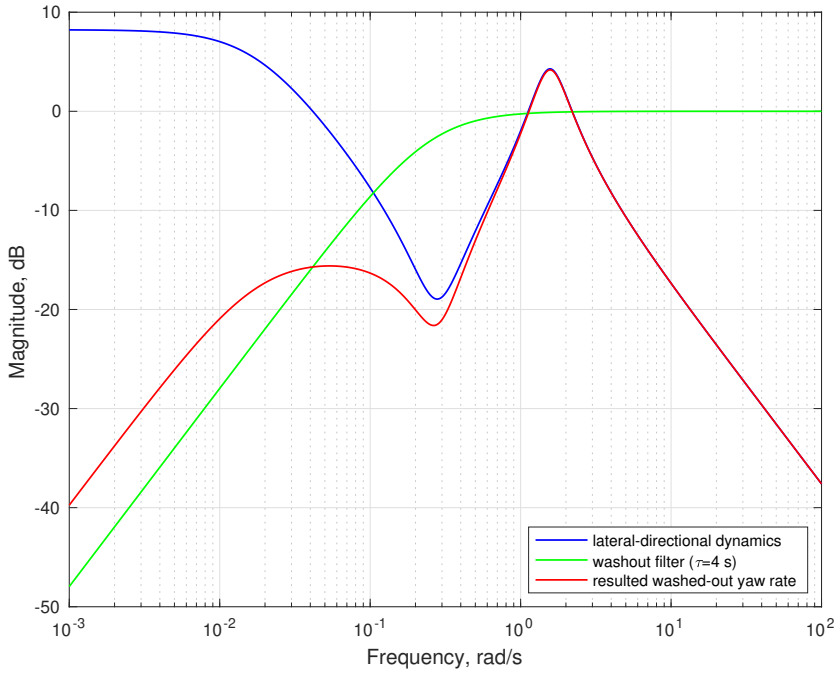

Fig. 17 Bode diagram of lateral-directional dynamics, washout filter, and the resulted washed-out yaw rate.

In the presence of washout filter, the feedback gain of the yaw damper must be recomputed using root locus technique for the desired Dutch roll damping ratio of 0.7. Notice that due to the washout filter zero at the origin of the complex plane, the spiral mode can no longer be stabilized by this feedback as in Subsection V.A. The new gain value, $K_{r\delta_r}$, is −0.92.

C. Verification

In a steady, horizontal turn, the lift vector will be divided into two components: a vertical component that counteracts the gravitational force, and a horizontal component directed into the turn that provides the required centripetal force. This centripetal force will create a negative sideslip angle assuming positive aileron input (right wing up). Additionally, for most of the conventional aircraft, a positive aileron input will result in a positive yawing moment (nose right). This yawing moment away from the direction of the turn results from the differential induced drag. With the induced drag higher on the wing coming up, a yawing moment away from the direction of the turn is generated [3]. The sideslip angle will become even more negative. This aerodynamic effect is called adverse yaw. During the coordinated turn, the pilot must accordingly apply a rudder deflection to compensate this effect.

Several control methods for the turn coordinator are proposed by Yedavalli [4]. To maintain controller simplicity, the sideslip-angle-to-rudder feedback is implemented, in which rudder deflection will respond to nonzero sideslip angle. Notice that another controller, called turn compensator, must also be implemented. This controller provides coupling between lateral-directional and longitudinal stability augmentation systems to maintain constant altitude during steady, horizontal turns. However, the design of this compensation system is beyond the scope of this paper. The block diagram of the lateral-directional SAS is presented in Fig. 18.

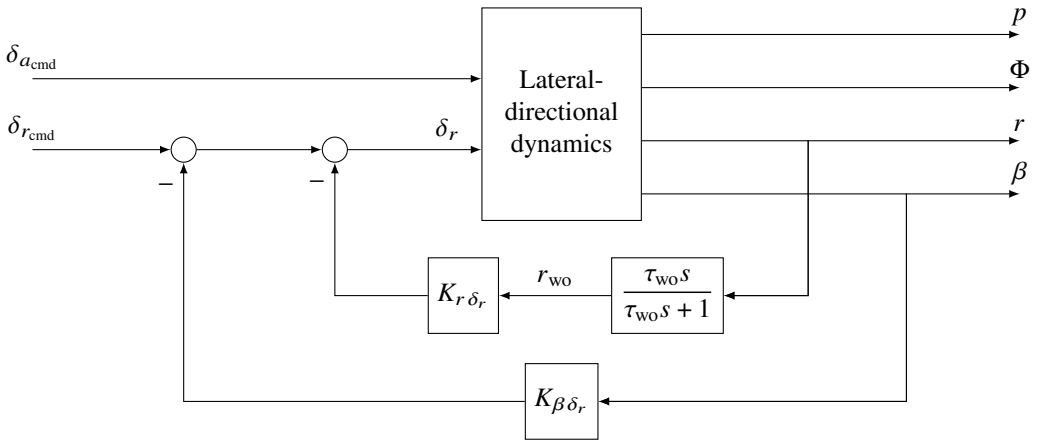

Fig. 18 Lateral-directional SAS.

The MIMO system requires an iterative design process when using root locus technique. To keep the Dutch roll damping ratio at 0.7 and also improve the turn coordination, we must redesign the yaw damper. This tedious iterative process can be replaced by modern control technique, such as pole placement. With some trial and error, the components for the lateral-directional SAS are determined as shown in Table 8. Notice that without integral controller the sideslip angle will not reach zero at the steady state. The control objective is to minimize the sideslip angle during turns using only proportional controller while maintaining a Dutch roll damping ratio of 0.7. Figure 19 illustrate the improvement in sideslip angle response to the aileron step input of 5°. The designed lateral-directional SAS demonstrates significant

performance improvement, as illustrated in Fig. 20. Notice that the path from aileron to the plant outputs is an open-loop system, see Fig. 18. This implies that aileron deflections under pilot control is directly the system input.

Table 8 Lateral-directional SAS.

Washout filter time constant	$\tau_{\text{wo}} = 4\,\text{s}$
Yaw damper	$K_{r\delta_r} = -1.43$
Turn coordinator	$K_{\beta\delta_r} = 1.352$

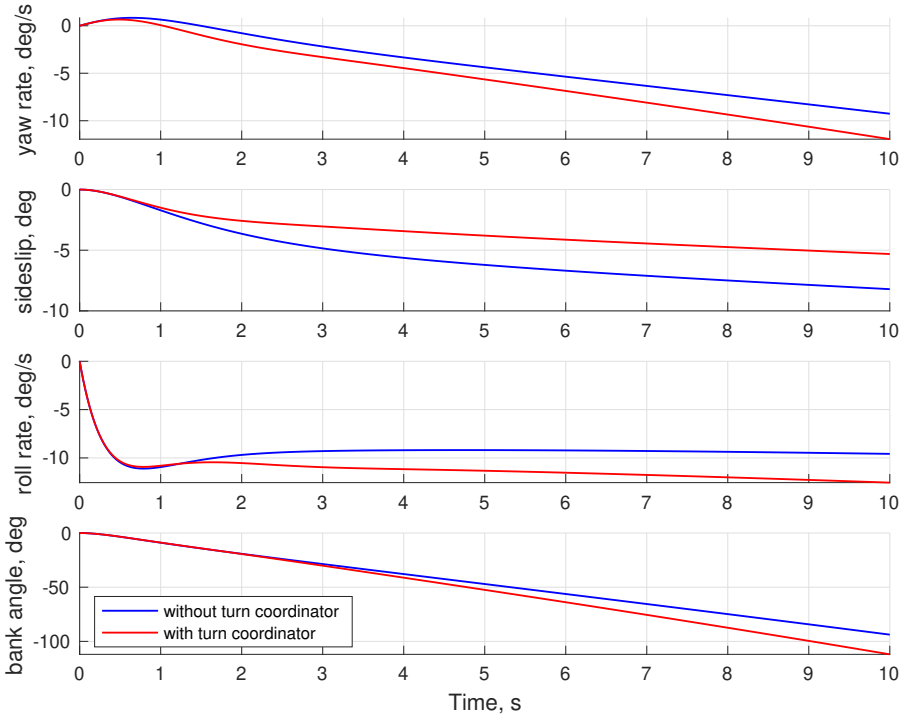

Fig. 19 Comparison of step response with and without turn coordinator.

VI. Testing the controllers in the nonlinear simulation

A. Nonlinear versus linear simulation

Practical systems inherently exhibit nonlinear behavior, in which the superposition principles is not applied. Therefore, a nonlinear dynamical system, $\dot{\boldsymbol{x}} = \boldsymbol{f}(\boldsymbol{x}, \boldsymbol{u})$, will introduce high level of complexity into system analysis and controller synthesis. Often, engineers will linearize a nonlinear system around some equilibrium points, which are defined as the points at which the system, without any disturbances, will stay perpetually, or $\dot{\boldsymbol{x}} = \boldsymbol{0}$. In the context of flight mechanics and control, these points are our defined trim conditions. Linearization is performed by applying Taylor

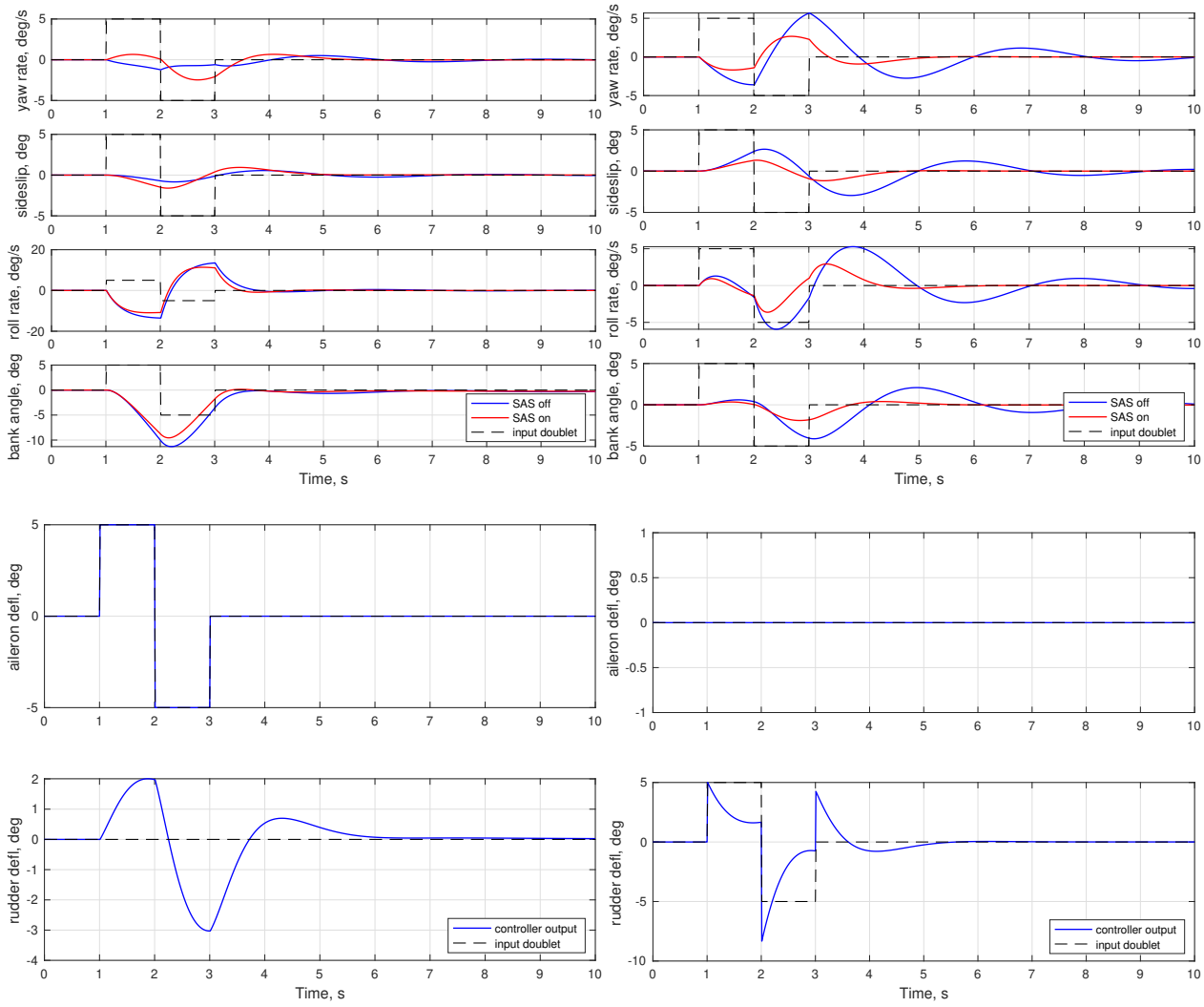

(a) Aileron doublet input. **(b) Rudder doublet input.**

Fig. 20 Comparison of doublet responses and controller output with SAS on and off.

series expansion to the system's differential equations around the trim condition and keeping only the linear terms, i.e.,

$$\boldsymbol{f}(\boldsymbol{x}_{\text{trim}} + \delta\boldsymbol{x}, \boldsymbol{u}_{\text{trim}} + \delta\boldsymbol{u}) = \boldsymbol{f}(\boldsymbol{x}_{\text{trim}}, \boldsymbol{u}_{\text{trim}}) + \left.\frac{\partial \boldsymbol{f}}{\partial \boldsymbol{x}}\right|_{\boldsymbol{x}=\boldsymbol{x}_{\text{trim}}} \cdot \delta\boldsymbol{x} + \left.\frac{\partial \boldsymbol{f}}{\partial \boldsymbol{u}}\right|_{\boldsymbol{u}=\boldsymbol{u}_{\text{trim}}} \cdot \delta\boldsymbol{u} + O(\|\delta\boldsymbol{x}\|_2^2, \|\delta\boldsymbol{u}\|_2^2) \tag{57}$$

Eliminating the higher-order terms and defining $\delta\dot{\boldsymbol{x}} = \boldsymbol{f}(\boldsymbol{x}_{\text{trim}} + \delta\boldsymbol{x}, \boldsymbol{u}_{\text{trim}} + \delta\boldsymbol{u}) - \boldsymbol{f}(\boldsymbol{x}_{\text{trim}}, \boldsymbol{u}_{\text{trim}})$, we obtain the linearized differential equations

$$\begin{aligned} \delta\dot{\boldsymbol{x}} &\approx \underbrace{\left.\frac{\partial \boldsymbol{f}}{\partial \boldsymbol{x}}\right|_{\boldsymbol{x}=\boldsymbol{x}_{\text{trim}}}}_{=\boldsymbol{A}} \delta\boldsymbol{x} + \underbrace{\left.\frac{\partial \boldsymbol{f}}{\partial \boldsymbol{u}}\right|_{\boldsymbol{u}=\boldsymbol{u}_{\text{trim}}}}_{=\boldsymbol{B}} \delta\boldsymbol{u} \\ &= \boldsymbol{A}\delta\boldsymbol{x} + \boldsymbol{B}\delta\boldsymbol{u} \end{aligned} \tag{58}$$

The linearized system only holds if the initial conditions and the state as well as the input variables are in the vicinity of the trim points. During the flight, aircraft's state and input variables will change from one trim condition to the other. Thus, the state and input variables will diverge, and the state space equation linearized around this trim point may not be valid for others. In this case, a set of different state space equations linearized at different trim conditions for different flight phases must be derived. Data between each condition will be interpolated to ensure smooth transition. The controller gains may be stored, for example, in a lookup table for later computation. This control method is called gain scheduling.

B. Evaluation of flight test results

To test the controller designed in Section IV.C for the longitudinal motion, we simulate a climb manouver with a steady climb rate of 1000 ft/s from an altitude of 4000 ft to 6000 ft. At its original state space, the fingerprint plot as shown in Figure 3 gives the information that the current aircraft has a poor control in short-period mode against a disturbance or certain changes. With the result of the simulation in Figure 21, we can derive that the the pilot can maintain a better and more steady rate of climb. There are also less oscillations occured in the Angle-of-Attack as the aircraft was approaching the target altitude of 6000 ft, which can be traced back to the integrated controller applied in Section IV.C. In general, the pilot can achieve a better result for the given climb manouver.

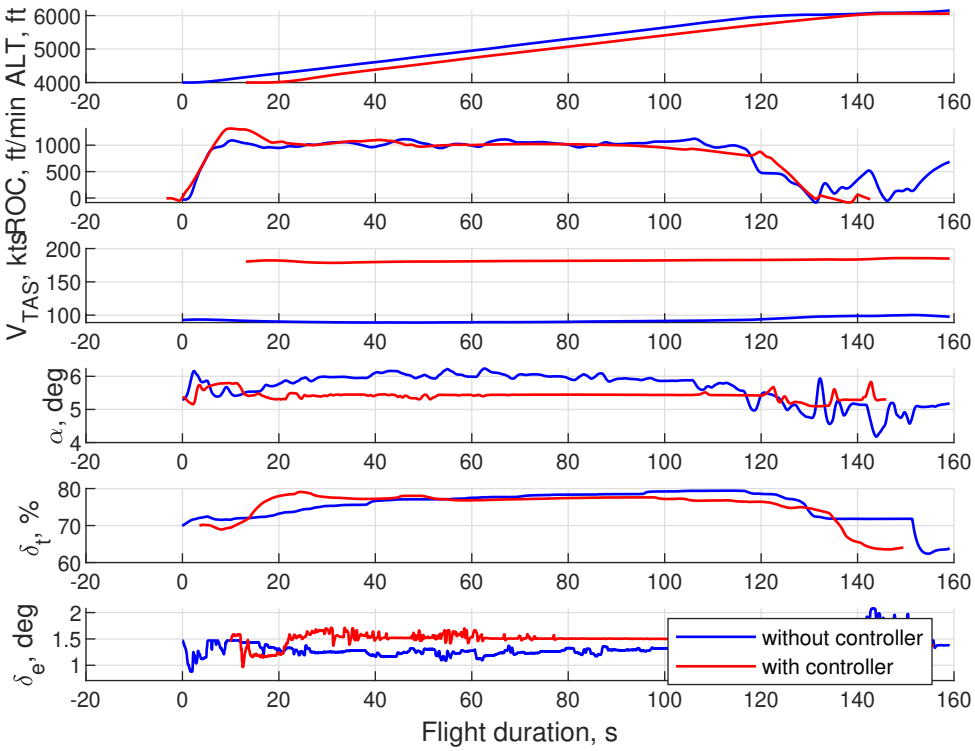

Fig. 21 SEPHIR simulation: longitudinal motion state variables.

Since VFW 614 already possesses good lateral-directional characteristics, as shown in Section III, the pilot had a little to no difficulty in conducting the standard rate turn. A standard rate turn is defined as a turn with a rate of $3\,^{\circ}/\mathrm{s}$, which completes a 360°-turn in 2 minutes. The required bank angle can be calculated from the turn rate in advance of the simulation session as follows

$$\tan(\phi) = \frac{V^2}{gR} \tag{59}$$

where ϕ is the required bank angle, v is the true airspeed, which is equal to trimmed speed, R is the radius of turn, and g is acceleration due to gravity. The relation between radius of turn, true airspeed and rate of turn, ω, is

$$R = \frac{V}{\omega} \tag{60}$$

Substituting this in Eq. 59 and solving for the bank angle, we obtain

$$\phi = \tan^{-1} \frac{V\omega}{g} \tag{61}$$

Thus, the required bank angle for a standard rate turn is approximately 26°.

As shown in Fig. 22, the state variables during the simulation between open loop and closed-loop system mostly coincide. A nonzero sideslip angle during the turn, which is improved through SAS implementation, can be easily observed. This result agrees with our simulation of linearized system.

Figure 23 illustrates the 2-minute standard rate turn with the heading angles unwrapped. The 360°-turn maneuver exceeded the allowed maximum duration, which is 2 minutes and 10 seconds. However, considering the transition time needed for the aircraft to from trimmed, level flight to reach the required bank angle, the requirement can still be considered satisfied.

During the horizontal turn, we must keep true airspeed and altitude constant. Figure 24 shows that with the SAS activated, the pilot can keep the true airspeed and altitude close to the trimmed point, in spite of some oscillations. Note that the pilot, with limited flying experiences, underwent task saturation when managing multiple flight parameters simultaneously. The observed oscillations resulted from continuous corrective inputs across multiple axes, including bank angle, airspeed, and altitude control.

The control surface deflections are shown in Fig. 25. Because aileron deflection commanded by the pilot is directly the system input, we can observe that the pilot continually corrected the bank angle in a small amount of stick control. With SAS activation, the rudder exhibited appropriate response characteristics. During right turn (increasing heading, see Fig. 23), the adverse yaw generates positive sideslip angles, requiring negative rudder deflections for compensation.

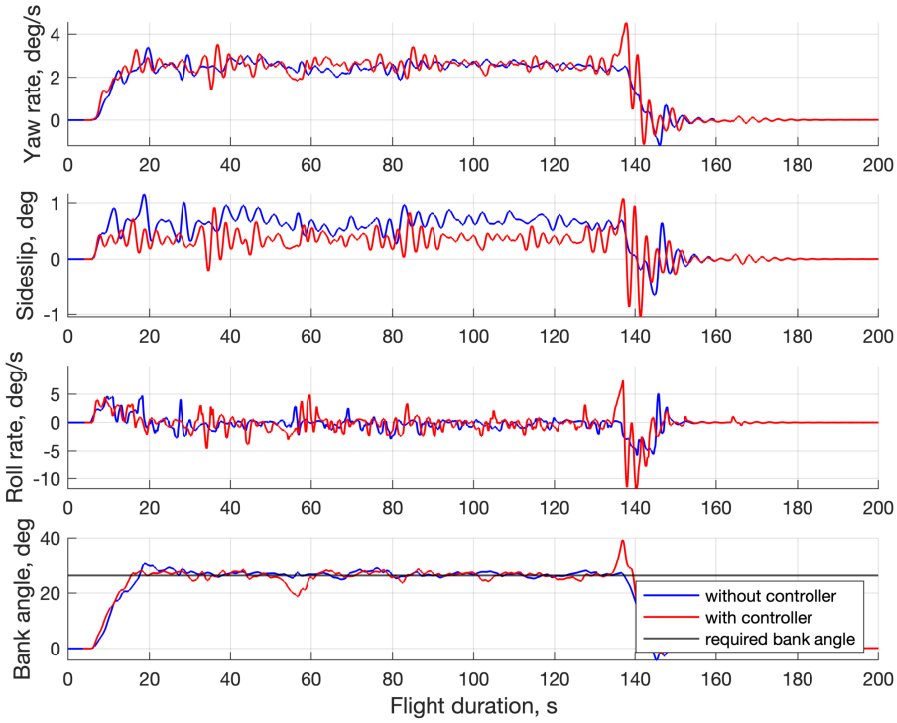

Fig. 22 SEPHIR simulation: lateral-directional state variables.

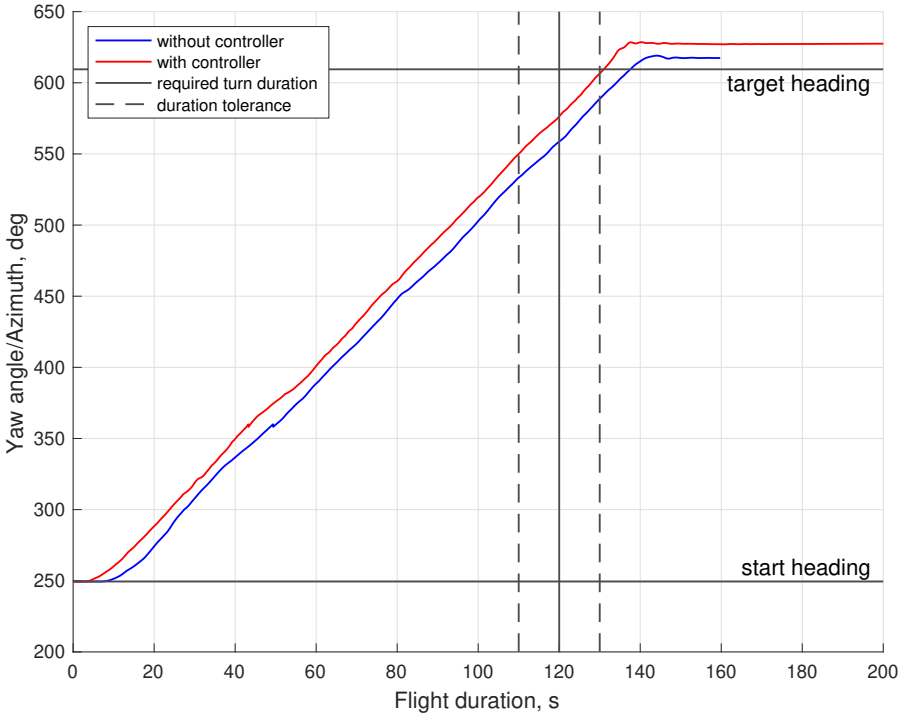

Fig. 23 SEPHIR simulation: Euler yaw angle/azimuth.

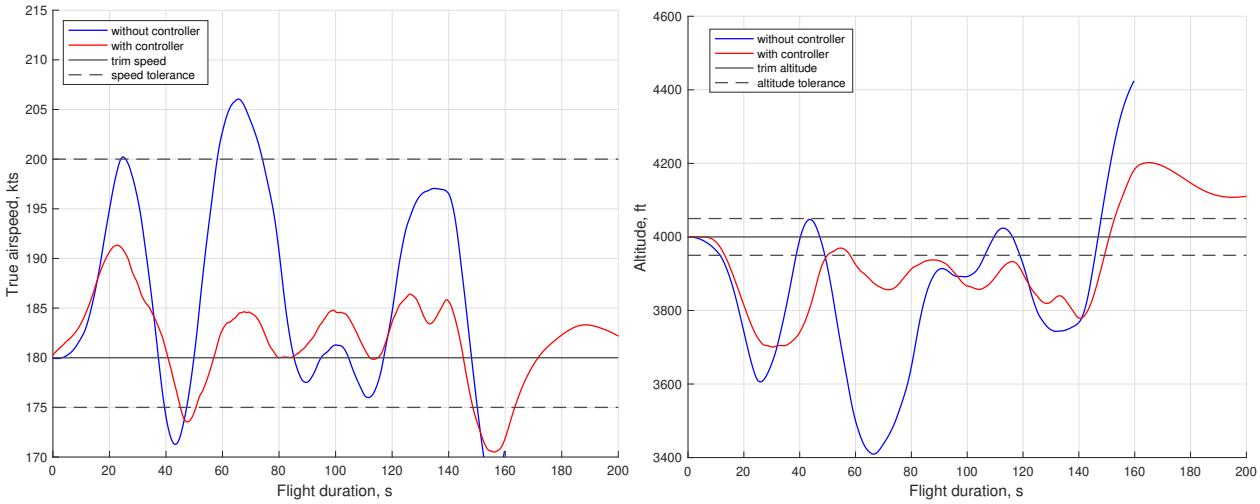

(a) True airspeed. **(b) Altitude.**

Fig. 24 SEPHIR simulation: true airspeed and altitude compared with trim condition.

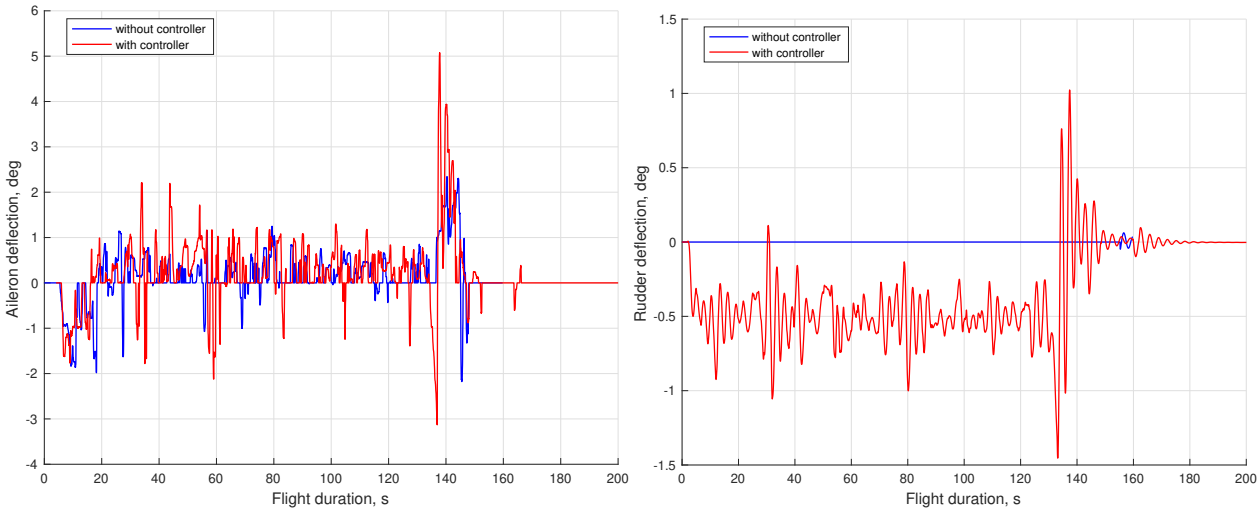

(a) Ailerons deflection. **(b) Rudder deflection.**

Fig. 25 SEPHIR simulation: control surfaces deflection.

VII. Conclusion

With the given aircraft state space, we have analyzed its original flying qualities through different plots. Through the plots, we could categorize to which level of control does the aircraft possessed. In certain area, like the short-period mode, the aircraft have a poor level of control. As for level of control in lateral motion, a satisfactory level is already achieved. Since we want to have the best flying quality, the current system should be improved. Through the improvisations done in Section IV and Section V, we can see the development of the state variables in a better way as seen in the results of the SEPHIR simulations.

References

[1] *Military Specification, Flying qualities of piloted airplanes, MIL-F-8785C*, United States Military Standard, 1980.

[2] Stevens, B. L., Lewis, F. L., and Johnson, E. N., *Aircraft Control and Simulation: Dynamics, Controls Design, and Autonomous Systems*, 3rd ed., John Wiley & Sons, Ltd, 2015, p. 295. https://doi.org/10.1002/9781119174882.

[3] Yechout, T. R., *Introduction to aircraft flight mechanics: Performance, static stability, dynamic stability, classical feedback control, and state-space foundations*, 2nd ed., American Inst. of Aeronautics and Astronautics, 2014, pp. 236, 237. https://doi.org/10.2514/4.102547.

[4] Yedavalli, R. K., *Flight Dynamics and Control of Aero and Space Vehicles*, Aerospace Series, John Wiley & Sons, 2020, pp. 265, 266.

Appendix

TESTKARTEN FLUGREGELUNG

Flugzeugtyp: VFW-614	**Datum:** 06.12.2024
Tail No.:	
Instrumentierung: Fixed-seat simulator	
Beteiligte Einrichtungen:	
Testfrequenz: 1	
Besatzung/Call Sign(s): H. N. Tang, Nauval, H. Nenijian	
Ziel des Testes: Testing the flight controllers in the nonlinear simulation	**Flugtestplan:** **Freigabe:** **Auftrag: TU Berlin**
Konfiguration beim Start:	

QNH:	OAT:	Rel Feuchte:	Wind:	Piste:

Testbeginn: 14:00 **Abheben:** 14:30 **Landung:** 15:30 **Flugdauer:** 1h	**Erfolgsquote:** ☐ Erfolgreich ☐ Nicht erfolgreich ☐ Teilweise erfolgreich ___%

TESTKARTEN FLUGREGELUNG

(Logo)

Erstellt von: _____
FVI: _____
Testleiter: _____
Pilot 1: _____
Pilot 2: _____
Pilot 3: _____

(weitere Beteiligte je nach Test)

Notizen vom Debriefing:

TESTKARTEN FLUGREGELUNG

LIMITIERUNGEN	SEITE A

1. Allgemeine Limitierungen

Trim condition: H = 4000 ft (1219 m), V = 180 KTAS (92.6 m/s, 303.81 ft/s), landing phase.

2. Testspezifische Limitierungen

Max. deviations for climb:

- Sink and climb rate: 200 ft/s.
- Height: 50 ft.
- Speed: -5 kt to 20 kt. => 175 to 200 kt

Max. duration deviation for standard rate turn: ±10 s.

3. Testspezifische Gefährdungsanalyse

Unspecified.

4. Wetterminima

No wind.

(weitere Informationen nach Bedarf, z.B. zulässige Enveloppe, optionale und unverzichtbare Einrichtungen, etc.)

TESTKARTEN FLUGREGELUNG

TESTKARTEN FLUGREGELUNG

TESTBESCHREIBUNG	SEITE 1

1. CLIMB

1.1. OPEN LOOP (WITHOUT CONTROLLER)

FROM TRIM (4000 FT), KEEPING THE SPEED CONSTANT BY USING THRUST, CLIMB TO 6000 FT, AT A RATE OF 1000 FT/M.

-> CLIMB FOR 2 MIN.

NOTE:

THROTTLE 68% STRAIGHT, 77% CLIMB

PILOT COMMENT: AIRCRAFT ACTS MORE SENSITIVE.

TESTKARTEN FLUGREGELUNG

1.2. CLOSED LOOP (WITH CONTROLLER)

REPEAT THE PROCEDURE.

NOTE:

PILOT COMMENT FOR BOTH:
CLEARLY MORE STABLE

TESTBESCHREIBUNG	SEITE 2

2. 2-MIN STANDARD RATE TURN

2.1. OPEN LOOP (WITHOUT CONTROLLER)

START A TIMER.

FROM TRIM, PERFORM STANDARD RATE TURN, 3°/S => 360° IN 2 MIN.

KEEP ALTITUDE CONSTANT AT 4000 FT, BANK ANGLE CONSTANT AT APPROX. 26°.

AFTER 2 MIN, END TIMER.

NOTE:

DURATION: 2 MIN 9 SEC FOR 360° TURN (1ST TRY)
2 MIN 8 SEC FOR 360° TURN (2ND TRY)

PILOT CONSTANTLY HAS TO CORRECT THE TURN AND ALTITUDE.

TESTKARTEN FLUGREGELUNG

2.2. CLOSED LOOP (WITH CONTROLLER)

REPEAT THE PROCEDURE.

NOTE:

DURATION: 1MIN 58 SEC

STILL HARD TO KEEP ALTITUDE CONSTANT DURING THE TURN (EASY TO UNDERSTAND BECAUSE NO TURN COMPENSATOR).

IT'S HARD TO KEEP ALTITUDE CONSTANT.